The circumnuclear gas and dust environment
of the ringed Seyfert 2 galaxy Mkn 620

I.M. Yankulova

Department of Astronomy, Faculty of Physics, St Kl. Okhridski University of Sofia, 5 James Bourchier Street, BG-1164 Sofia, Bulgaria
(Yan@phys.uni-sofia.bg)

Abstract. We present here new flux-calibrated narrow-band images of the circumnuclear region of the Seyfert 2 galaxy Mkn 620 = NGC 2273 in the light of [O III]λ4959 Å, [O I]λ6364+[Fe X]λ6374 ÅÅ and [N II] λ6548 Å emission lines and two continuum images at λ6300 Å and λ4260 Å, and in a broad band Gunn r continuum.

The color map $F_\lambda(6300\,\text{Å})/F_\lambda(4260\,\text{Å})$ reveals a dusty ring-like structure around the nucleus of Mkn 620. This ring-like structure has a diameter of about 14 arcsec corresponding to $\approx$ 1700 pc. Its mean projected thickness is about 500 pc and it is much more prominent in the north-west direction from the nucleus.

The dusty ring-like structure surrounds a zone of high ionization which is represented by the [O III]λ4959 Å contour map. The [N II] λ6548 Å and [O I]λ6364 Å emissions are visible both in the inner high ionized zone and in the outer partially ionized zone (PIZ), which coincides with the dusty ring.

Based on the color map $F_\lambda(6300\,\text{Å})/F_\lambda(4260\,\text{Å})$ we have estimated an extinction of $A_V = 1^m04$ which yields $10^5 \times \text{M}_\odot$ for the mass of the dust in the ring. This dust mass would be able to produce the observed 12 and 25 μm emission if the equilibrium dust temperature T_d is larger than 110 K. This value is determined by the equilibrium between the absorbed and emitted energy, assuming thermal dust reemission of the nonthermal AGN continuum. Both larger nonthermal ionizing flux and star formation events in the innermost circumnuclear region could result in higher equilibrium dust temperature T_d.

A second dusty ring is clearly seen on the color map. Its radius is $\approx$ 20 arcsec (2.4 kpc) and is approximately placed on the inward side of an ovally distorted disk.

Key words: galaxies: individual: Mkn 620 = NGC 2273 – galaxies: ISM – galaxies: Seyfert – galaxies: structure

1. Introduction

In recent years, several arguments have been advanced to indicate that galaxy interactions and/or orbital resonances can lead to the enhanced fueling of various kinds of nuclear activity, especially the Seyfert and Starburst phenomena (Heckman 1990, 1991; Dultzin-Hacyan, 1997). Particularly interesting in this respect are Seyferts with rings and bars. The common ringed galaxies are believed to outline the locations of major orbital resonances with a bar or oval distortion in the galactic disk (Buta 1986ab, Norman 1987).

In the theory of AGNs the luminous ($L_{IR} > 10^{10} L_\odot$) IRAS galaxies play an important role. It appears that the luminous IR galaxies are extraordinarily rich in molecular hydrogen, highly concentrated towards their nuclei (Scoville & Soifer 1991; Scoville et al. 1994). This matter reservoir plays a central role in promoting star formation and possibly fueling accretion onto the central compact object (Scoville et al. 1991).

Studies of dust and gas distribution in the circumnuclear regions of luminous IRAS AGNs galaxies with rings and bars provide information both about the link between the AGN and star formation events and about the matter transport to the active nucleus.

NGC 2273 (Mkn 620) was discovered by Huchra et al.(1982) to be a type 2 Seyfert galaxy and classified by de Vaucouleurs et al., 1991 [RC3] as a morphological type SB(r)a:. The heliocentric recession velocity is $cz = 1875$ km sec^{-1} [RC3].

According to van Driel & Buta (1991) this galaxy shows faint doubled outer ring-like structure, which consists of two incompletely closed concentric structures formed by separated sets of spiral arms at radii of 7.3 and 10.2 kpc. There is foreshortened bar and an inner ring-like shaped by sets of spiral arms.

NGC 2273 has been detected by IRAS (Lonsdale et al., 1992 hereafter LLS92) with strong far infrared emission (FIR) $L_{FIR} \sim 10^{10} L_\odot$.

Young & Devereux (1991) have presented new CO 2.6 mm observations of Mkn 620 and determined the mass of molecular gas confined to the central 45 arcsec to be $M(H_2) \approx 2.8 \times 10^9$ M$_\odot$. The CO line width is found to be less than 260 km s^{-1} and this may indicate that the molecular gas is confined to the central few arcseconds in this galaxy. The star formation rate per unit mass of molecular gas in the nucleus of Mkn 620 is $L_{IR}/M(H_2) \approx 8.7$.

The mid-infrared emission of Mkn 620 at 10 μm measured by Devereux (1987) in small aperture ($\sim$ 5 arcsec) is due to thermal dust reradiation of the UV/optical emission of the central source (Giuricin et al.,1995).

The continuum measurements by Krugel et al. (1988) at 1300 μm and the spectral index between 100 and 1300 μm

clearly indicate that the emission must be thermal reradiation from dust.

CCD interference-band images isolating the emission lines of Hα + [N II]$\lambda\lambda$6548/84 ÅÅ and [O III]λ5007 Å were obtained by Pogge (1989) and Mulchaey, Wilson and Tsvetanov (1996) (hereafter MWT96) to search for spatially extended circumnuclear emission regions.

In this paper we present the results of new narrow and broadband imaging to study gas and dust distribution in the circumnuclear region of the ringed Seyfert 2 galaxy Mkn 620. Some information on the observations and data reduction procedures is presented in Sect. 2. The results are given and analyzed in Sects. 3 and 4, respectively. Their compatibility with the IR measurements is discussed.

2. Observations and data reduction

2.1. Observations

Mkn 620 was observed with the 2m Ritchey-Chretien-Coudé (2-m RCC) reflector of the Bulgarian National Astronomical Observatory (BNAO) at Mount St. Spirit near Rozhen, Rodopa mountains. The observations were carried out on December 12, 1992.

The narrow-band images were taken with the Focal Reducer of the Max-Planck-Institute for Aeronomy (MPAe). The technical data and the capabilities of the MPAe Focal Reducer are described by Jockers (1992).

The telescope / reducer configuration and the CCD's square 22 μm pixels provide an image scale of $0\overset{''}{.}8$ px^{-1} and an unvignetted field of view (FOV) $\sim$ 7×5 arcmin at an effective focal ratio f/2.86. This scale is quite well adapted to the typical seeing conditions at BNAO ($2''-2\overset{''}{.}5$ FWHM). One arcsec corresponds to a distance of 125 pc at Mkn 620 assuming $H_o = 75$ km sec^{-1} Mpc^{-1}.

Images through interference filters centered near the wavelengths of [N II] λ6548 Å,[O III]λ4959 Å and [O I]λ6364+[Fe X]λ6374 ÅÅ ("on-line") and on the emission free continuum windows at λ4260 Å and λ6300 Å ("off-line") were obtained. The "off-line" images were used to subtruct the continuum contribution contained in the "on-line" images. Moreover, we utilized the "off-line" images to form the color map.

A broad band image was also obtained with a Gunn r interference filter.

The observing log is presented in Table 1 where the central wavelengths λ_c and the effective width $\Delta\lambda$ of the interference filters, and the spatial resolution of the images in terms of the point-spread function (PSF) are listed.

Two exposures of Mkn 620 were obtained through each filter to eliminate cosmic ray events and to increase the reliability of the measurements. Between exposures the telescope was slightly offset to avoid permanent defects of the CCD. Flatfield exposures were obtained using dusk and dawn twilight for uniform illumination of the detector. No dark correction was required.

Table 1. M 620-observing log and related data.

image frame	interference filter, $\lambda_c/\Delta\lambda$	exposure time	final FWHM resolution
	(Å)/(Å)	(s)	(arcsec)
[N II] λ6548	6567/30	1×300	4.4
[O I]λ6364+[Fe X]λ6374	6420/30	2×300	3.2
red continuum	6300/34	2×300	3.2
[O III]λ4959	5003/40	2×300	2.7
blue continuum	4260/34	2×300	3.1
Gunn r	6550 /900	2×300	4.3

2.2. Data reduction

The images were reduced following the usual reduction steps for narrow-band imaging (Haniff et al. 1988; Perez-Fournon & Wilson 1990; Tsvetanov & Walsh 1992).

The raw images contained a small amplitude pattern, periodic along the rows. Analysis of the overscanned area showed that a pattern with the same amplitude and phase existed therein. Therefore it was possible to use the overscan for creating bias frames with the systematic additive noise, characteristic for each particular image. Afterwards the bias and periodic pattern have been removed in one step.

After flat-fielding the frames were aligned by rebinning to a common origin. The final alignment of all the images was estimated to be better than $0\overset{''}{.}1$. As an unwanted by-product of the rebinning procedure a small decrease of the resolution ($\sim 0\overset{''}{.}15$) was noticeable. The two images taken through the same filter were averaged and the cosmic-ray signatures were removed.

Unfortunately, small tracking errors of the 2-m RCC telescope caused residual ellipticities in the PSFs of our frames. Therefore, a convolution procedure was performed in order to match the PSFs of each line–continuum pair. The same procedure was applied to those images which later were used in the mapping of continuum emission ratios. This degraded the final resolution to a mean value of $\sim 3\overset{''}{.}3$.

3. Results

3.1. Broad and narrow-band continuum images

Contour map of the broad band r continuum is presented in Fig. 1. Several morphological features are clearly seen: the outermost ring-like structure at radius of 7.3 kpc ($\approx$ 60 arcsec); an ovally distorted disk with a radius of about 30 arcsec. The innermost visible structure is a bar with P.A.$\approx 114°$. Weak spiral arms originate from the bar and form an inner ring-like with radius $\approx$ 2.4 kpc (20 arcsec). Similar features are noted and discussed by Gallagher & Wirth (1980) and van Driel & Buta (1991).
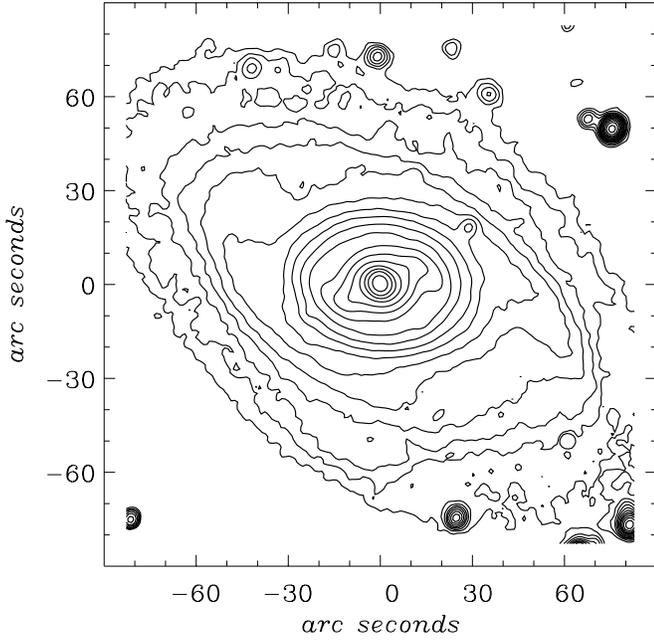
Fig. 1. Contour plot of the Gunn r image. The outermost contour is at $2\,\sigma$ of the background ($1\,\sigma$ background noise level is 3×10^{-18} ergs cm^{-2} s^{-1} arcsec^{-2}Å^{-1}). Next contours increase as a power series of 2
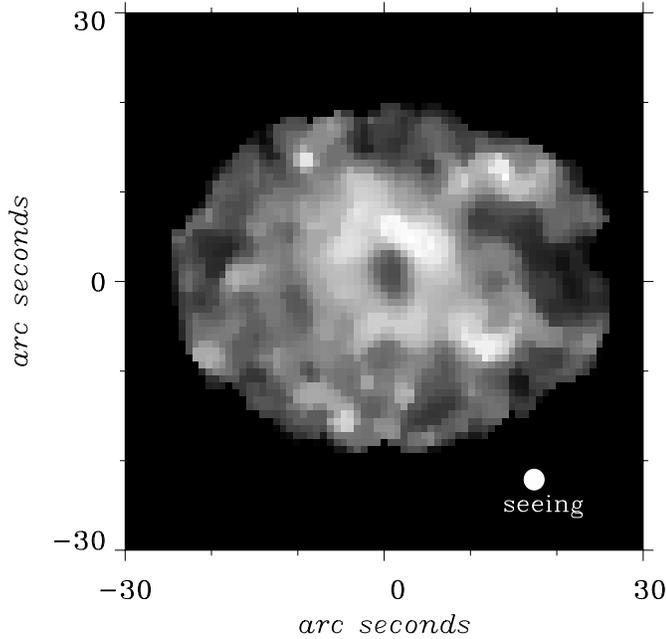
Fig. 2. Red/blue narrow-band color map of Mkn 620

It should be noted, the Gunn r continuum contour map (Fig. 1) shows an isophotal twist in the innermost region of Mkn 620. Similar isophotal twists are observed in early type spirals and could be associated with inner Lindblad resonances (ILR) (Elmegreen & Elmegreen 1996).
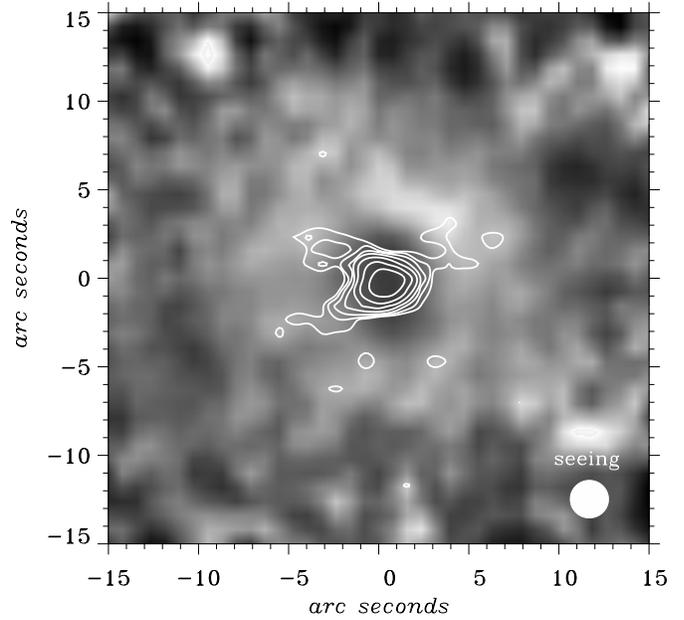
Fig. 3. The [O III]λ4959 Å-emission contours superimposed over the red/blue narrow-band color map

The continua images obtained at $\lambda\,4260$ Å and $\lambda\,6300$ Å were used to create the narrow-band color map presented in Fig. 2, where "black" means excess of light while "white" means absorption. The color map reveals an inner redder structure reminding of dusty ring around the AGN nucleus of Mkn 620. This ring-like structure has a diameter of about 14 arcsec corresponding to ≈ 1700 pc. Its mean projected thickness is about 500 pc. The dusty ring is disconnected in the east-west and it is much more prominent in the north-west of the nucleus.

A second dusty ring is clearly seen on the color map. It is approximately placed on the inward side of the ovally distorted disk and its radius is ≈ 20 arcsec (2.4 kpc). Gallagher & Wirth (1980) have also shown the presence of outer rather red ring.

We calibrated the continuum image in F 426 and estimated the observed flux $F_\nu(4260\,\text{Å}) = 3.32 \times 10^{-26}\text{ergs cm}^{-2}\text{s}^{-1}\text{Hz}^{-1}$. On the other hand, according to Rowan-Robinson & Crawford (1989) the starburst and Seyfert components for Mkn 620 contain 0.74 of the whole infrared emission. We utilize this value to estimate the nonthermal AGN fraction of the observed flux. The later was used to calculate the energy density of the radiation field in the circumnuclear region occupied by the dusty ring.

3.2. Narrow-band emission line images

The emission line contours of [O III]λ4959 Å, [N II] λ6548 Å and [O I]λ6364+[Fe X]λ6374 ÅÅ superimposed on the $F_\lambda(6300\,\text{Å})/F_\lambda(4260\,\text{Å})$ color map are presented in Fig. 3 and Fig. 4. The corresponding $1\,\sigma$ background noise levels in the emission line images are presented in Table 2. The lowest isophotal level is at $3\,\sigma$ above the sky subtraction level and the following contours are multiplied with $\sqrt{2}$.
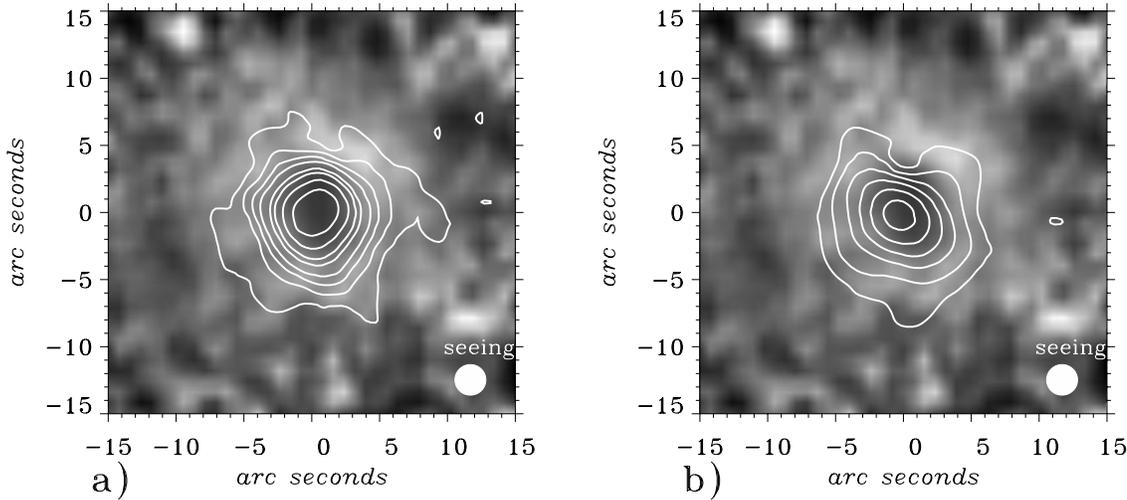
Fig. 4. a The [N II]$\lambda6548$ Å emission contours superimposed over the red/blue narrow-band color map; **b** The [OI]$\lambda6364$ + [FeX]$\lambda6374$ ÅÅ emission contours over the same color map

The [O III]$\lambda4959$ Å emission arises entirely in the circumnuclear region enclosed by the dusty ring and it is strongly reduced there where the dust content is enhanced.

The [N II] $\lambda6548$ Å emission (Fig. 4a) shows extended structure in diameter of about 18 arcsec. The morphology does not differ from that of the Hα + [N II]$\lambda\lambda6548/84$ ÅÅ image presented by MWT96. The outermost contour in Fig. 4a is at 3σ above the noise level and includes entirely the dusty ring.

The [O I] emission is a good diagnostic tool for the presence of hard nonthermal ionizing photons. Both emission lines [O I]$\lambda6364$ Å and [Fe X]$\lambda6374$ Å (Fig. 4b) are transmitted through the F 642.

The Gunn r contours (Fig. 1), the color map (Fig. 2) and the presence of extended emission line regions suggest that the ionized region is a gaseous disk with an orientation of the major axis at P.A. $\approx 20°$. The gaseous disk wound by the dusty ring appears to be viewed at an inclination of $\sim 32°$ to the line of sight derived from the ratio of major to minor axes (Fig. 1).

The width of the dusty ring projected onto the sky plane is comparable with its geometrical depth due to the small inclination angle to the line of sight. Note that the inclination angle for the galaxy stellar disk is $\sim 45°$ (Whittle 1992; de Vaucouleurs et al.1991 [RC3]).

From our calibrated images we estimated the total fluxes of the observed emission lines in apertures used by other authors. Optical spectral observations of Mkn 620 were made by LLS92, and Ho, Filippenko & Sargent, 1997 (HFS97), where the slit width and length are (1.5×20) arcsec and (2.0×4.0) arcsec, respectively. We performed an integration of the fluxes inside these apertures and in aperture (14.0×16.5) arcsec used by MWT96. The data are presented in Table 2. Our measured fluxes in [O III]$\lambda4959$ Å and [N II] $\lambda6548$ Å agree quite well with the fluxes presented by LLS92 and are larger than that measured by MWT96. The transmission of H$\alpha\lambda6563$ Å in the interference filter F 657 Å centered near the wavelength of [N II] $\lambda6548$ Å is about 10% which results in a larger flux.

We have to note that the measured fluxes by HFS97 in emission lines of [O III]$\lambda4959$ Å and [N II] $\lambda6548$ Å in aperture $2'' \times 4''$ exceed the fluxes of the same lines measured in larger apertures by LLS92 and MWT96. But on the other hand, the authors in HFS97 have stated the photometric accuracy of the line fluxes are only approximate.

4. Discussion

4.1. Gas and dust in the narrow line region in Mkn 620

Previous studies of Mkn 620 have revealed a strong [O III]$\lambda5007$ Å emission concentrated around the nucleus and circumnuclear extended emission of Hα + [N II]$\lambda\lambda6548/84$ ÅÅ (Pogge, 1989; MWT96).

The color map $F_\lambda(6300\,\text{Å})/F_\lambda(4260\,\text{Å})$ (Fig. 2) infers the presence of a redder dusty ring-like structure around the AGN nucleus of Mkn 620. Otherwise, the innermost circumnuclear region is not influenced by extinction. We assume that the circumnuclear emission line region with diameter of about 700–800 pc, where the [O III]$\lambda4959$ Å contours are situated is a high ionized Strömgren zone (Fig. 3). The Strömgren depth is defined as

$$N_{H^+}^S = c\,\Gamma/\alpha_B \approx 10^{23}\,\Gamma \quad \text{cm}^{-2}, \tag{1}$$

where α_B cm^3 sec^{-1} is the recombination coefficient to excited states of hydrogen, c is the speed of light and Γ is the ionization parameter. In order to estimate Γ we take the electron density ≈ 600 cm^{-3} following LLS92. As was mentioned in Sect. 3.1, the nonthermal component of the ionizing continuum $F_\nu \approx \nu^{-\alpha}$ amounts 0.74 of the measured flux $F_\lambda(4260\,\text{Å})$. Taking a resonable value for $\alpha \approx 1.5$ we estimate the ionizing parameter $\Gamma \approx 10^{-3}$ which yields $N_{H^+}^S \approx 3.0\times10^{20}$ cm^{-2}.

The [N II] $\lambda6548$ and [OI]$\lambda6364$ + [FeX]$\lambda6374$ emissions (Fig. 4a,b) arise both in the inner Strömgren zone and in the dusty ring. Thus the redder dusty ring-like structure appears to be a large partially ionized zone (hereafter PIZ) in which the

Table 2. M 620-observed emission line fluxes in units of $\left(\frac{\text{ergs}}{\text{cm}^2\,\text{s}}\right)$

emission line (Å)	LLS92 spectral data in aperture of $1''.5 \times 20''$	our fluxes, in aperture of LLS92	MWT96 imaging data in aperture of $14''.1 \times 16''.5$	our fluxes, in aperture of MWT96	HFS97 spectral data in aperture of $2''.\times 4''.$	our fluxes, in aperture of HFS97	r.m.s. uncertainty
[O I]λ6364 + [Fe X]λ6374	–	10.14×10^{-15}	–	–	–	11.19×10^{-15}	0.036×10^{-15}
[O I]λ6364	5.0×10^{-15}	–	–	–	10.0×10^{-15}	–	–
[O III]λ4959	50.0×10^{-15}	44.88×10^{-15}	39.28×10^{-15}	50.64×10^{-15}	92.0×10^{-15}	36.86×10^{-15}	0.1×10^{-15}
[N II] λ6548	32.0×10^{-15}	36.82×10^{-15}	70.0×10^{-15}	98.35×10^{-15}	74.5×10^{-15}	42.12×10^{-15}	0.038×10^{-15}

The flux in [N II] λ6548 Å has been obtained assuming H_α/[N II] λ6548 Å/[NII] λ 6584 Å = 3/1/3.

ionized gas becomes neutral. The existence of this large PIZ results from harder photons of the ionizing continuum.

In our color map (Fig. 2 and see also Fig. 3) the Strömgren zone is homogeneous and we assume the measured flux ratio $F_{\lambda 6300}/F_{\lambda 4260} = 1.5$ is not reddened there. But in the PIZ, where the dust content is enhanced this ratio is influenced by dust extinction (absorption and scattering) and it is about 2.5. The dust opacity τ_λ^{dust} is given by

$$\tau_\lambda^{dust} = \mu\, N_{H^0}(PIZ)\,(\sigma/H), \qquad (2)$$

where σ/H (cm^2 per hydrogen nucleus) is the total extinction cross section and μ is the dust content of the medium expressed relative to the standart ISM dust-to-gas mass ratio (Binette et al. 1993). We assume $\mu = 1.0$ and take σ/H from Draine & Lee (1984) (see their Fig. 7). Based on the reddened and unreddened flux ratios $F_{\lambda 6300}/F_{\lambda 4260}$ we estimate the column density in the PIZ $N_{H^0}(PIZ) \approx 2.0 \times 10^{21}$ cm^{-2}. Then the total column density is

$$N_H^{slab} = N_{H^+}^S + N_{H^0}(PIZ) \approx 2.3 \times 10^{21} \text{cm}^{-2}. \qquad (3)$$

The column density N_H^{slab} defines the depth of the complete "photoexcited" region, that is the depth at which the incoming ionizing flux is exhausted.

The extinction opacity at 5500 Å is $\tau_V = 4.8 \times 10^{-22}\,\mu\,N_{H^0}(PIZ) = 0.96$ and the extinction is $A_V = 1.086\tau_V = 1^m.04$ if $\mu = 1.0$. Following Spitzer (1978) we can estimate the mean dust density along the line of sight

$$\rho_{dust} = 1.3\,10^{-27}\,\rho_s < A_V/L_{kpc} > \left(\frac{\epsilon_o + 2}{\epsilon_o - 1}\right),\text{g cm}^{-3} \quad (4)$$

where ρ_s is the density of the particular dust grains and we assume $\rho_s \approx 1.0$ g cm^{-3}. The dielectric dust function ϵ_o in the low frequency's limit is $\epsilon_o \approx 4$ (Spitzer 1978). The mean extent of the dusty ring-like structure measured on the color map is $L_{kpc} = 0.5$ kpc. Then according to Eq. (4) the mean dust density along the line of sight is $\rho_{dust} = 7 \times 10^{-27}$ g cm^{-3}.

From Fig. 2 we can roughly estimate the volume occupied by the dusty ring $\approx 4 \times 10^{64}$ cm^3 assuming a filling factor of ≈ 1. Knowing ρ_{dust} we determine the dust mass contained by

the observed dusty ring $M_{ring} \approx 1.5 \times 10^5$ M$_\odot$. This value is an upper limit since a filling factor of ≈ 1 was assumed.

Balmer decrement. The Balmer emission lines could be affected by the presence of PIZ in the circumnuclear region of Mkn 620. The measured Balmer decrement by LLS92 in Mkn 620 is $(H_\alpha/H_\beta)_{obs} \approx 7$. After a correction for the reddening we obtain a dereddened Balmer decrement ≈ 4.9.

Binette et al.,(1993) have shown the integrated Balmer lines of a power-law photoionized gas in a system of clouds with internal dust would be significantly affected because of dust and perspective. The same authors argue the intrinsic Balmer decrement could be as steep as 4–4.4 in the radiation bounded case where many clouds are seen from the back side.

4.2. Infrared emission of Mkn 620

The IRAS data show that Mkn 620 is a luminous IR galaxy $L_{\text{FIR}}(40 - 300\ \mu\text{m}) = 2.4 \times 10^{10} L_\odot$. The spectral indexes, defined as $\alpha(\lambda_1, \lambda_2) = -log(F(\lambda_2)/F\lambda_{(1)})/log(\lambda_2/\lambda_1)$ are $\alpha(12, 25) = -1.566$, $\alpha(25, 60) = -1.82$ and $\alpha(60, 100) = -0.80$ and place this galaxy in the typical range for Seyfert galaxies in the color-color diagram $\alpha(60, 100)$ versus $\alpha(25, 60)$ (Miley et al. 1985).

The main components of FIR emission are nonthermal AGN continuum continued to IR domain and thermal dust reemission. We favor the nonthermal UV continuum as the energy source which heats the dust.

The temperature of a dust particle is determined by the equilibrium between the absorbed and emitted energy

$$c \int_{\nu_1}^{\nu_2} Q_{abs}(\lambda)\,U_\nu\,d\nu = 4\pi \int_0^\infty Q_{abs}(\lambda)\,B_\lambda(T_d)\,d\nu\,, \qquad (5)$$

where

$$U_\nu = \frac{4\pi}{c}\left(\frac{R_g^2}{r^2}F_\nu\right) \qquad \text{ergs cm}^{-3}\text{Hz}^{-1},$$

is the energy density of the radiation field and $R_g \approx 25$ Mpc is the distance to the galaxy. The mean intensity $(R_g{}^2/r^2)F_\nu$

in ergs cm^{-2} s^{-1} Hz^{-1} of the radiation field at distance $r \approx$ 700 pc from the central nonthermal point source is obtained from the measured flux $F_\nu(4260\,\text{Å})$ extrapolating it to the UV with spectral index $\alpha = 1.5$. In Eq. (5) $\nu_1 = 3 \times 10^{14}$ Hz = 1 μm and $\nu_2 = 3 \times 10^{16}$ Hz = 100 Å are the assumed upper and lower limits to the frequencies which can heat the dust. $B_\lambda(T_d)$ is the Planck function at grain temperature T_d. The absorption efficiency $Q_{abs}(\lambda)$ in first approximation varies as $1/\lambda$ for a lot of dust particles in the visual and IR ranges (Spitzer 1978). Eq. (5) yields an equilibrium dust temperature $T_d = 110\,\text{K}$.

Most of the 12 and 25 μm emission in Seyfert galaxies is from dust in ionized gas, heated both by nonthermal AGN continuum and by stellar UV photons (Mouri & Taniguchi, 1992; Granato & Danese, 1994).

It is natural to speculate that the IR $\lambda < 30$ μm emission arises in the dusty ring-like structure inferred by the color map. Assuming dust thermal reradiation we make an estimation of the dust mass M_{dust} responsible for the observed IRAS flux F_{25}. Taking $T_d = 110\,\text{K}$ and the measured IRAS flux $F_{25\mu m} = 1.37$ Jy we derive $M_{dust} \approx 10^6$ M$_\odot$ if the dust particles consist of astronomical silicates, and $\approx 3 \times 10^6$ M$_\odot$ if the dust particles are graphites with small radii < 1 μm. The estimated dust mass depends on the dust temperature and is an order of magnitude greater than the value $M_{ring} \approx 10^5 \times$ M$_\odot$, obtained in Sect. 4.1 assuming that the observed extinction is entirely due to the dusty ring. If the T_d is larger than 110 K then the required dust mass, needed to explain the 25 μm flux, would be smaller. Both larger nonthermal ionizing flux and star formation events could result in higher dust temperature T_d. We have to note, that according to Young & Devereux (1991) Mkn 620 exhibits levels of nuclear star formation activity for radii less than 700 pc. Also there is a high 10 μm luminosity in the circumnuclear region (≈ 5 arcsec) of Mkn 620 which is an indication of nuclear star formation activity (Giuricin et al. 1995).

Dust ring-like morphologies. Dust ring-like morphologies in Seyfert galaxies could be traced both by red/blue color maps and by mid-infrared radiation. The 10.8 μm maps of the central region of the infrared-luminous barred galaxies NGC 1068 and NGC 1097 show the morphologies like kiloparsec-size rings which are intimately associated with the dense neutral interstellar gas inferred from CO maps (Telesco et al. 1993).

Moreover, in these two galaxies the observed dust ring-like morphologies coincide with the ILRs and demonstrate the role played by bars and oval distortions in the genesis of starbursts (Telesco et al. 1993).

If there are extended dusty clouds around Seyfert nuclei, they would show excess emission at FIR because the equilibrium temperature is about 100 K (Granato et al. 1996; Taniguchi et al.1997). In many objects, these dusty clouds are also connected with the occurrence of the circumnuclear starburst regions. Their typical radii range from several 100 pc to 1 kpc (Telesco et al. 1984; Boer & Schulz 1993; Genzel et al. 1995; Storchi-Bergmann et al. 1996). Arguments favoring the en-

hanced star formation around the nuclei of Seyfert galaxies as an alternative of the Unified model are presented by Dultzin-Hacyan (1995).

On the other hand, the accumulation of large amount of gas and dust near the ILR is connected with the supply of gas to the nucleus of Seyfert galaxy. Wada and Habe (1992;1995) have found a new fueling mechanism from kpc to several tens of pc, which is induced by a weak bar and the self-gravity of the gas in a massive gaseous disc. In their model the first ILR is essential for gas accumulation near the centre. The second ILR occupies, roughly, a diameter of about $\sim$ 1–2 kpc.

The dust ring-like structure ($\sim$ 1700 pc in diameter (Fig. 2)) observed in Mkn 620 could be associated with a shocked dust connected with the ILRs.

As a rule, the dust ring-like morphologies favore type 2 Seyfert galaxies which possess SB morphology.

References

Binette L., Wang J., Villar-Martin M., Martin P.G. Gladis Magris C., 1993, ApJ 414, 535

Boer B., Schulz H., 1993, A&A 277, 397

Buta R., 1986a, ApJS 61, 609

Buta R., 1986b, ApJS 61, 631

de Vaucouleurs G., de Vaucouleurs A., Corwin H.G., et al., 1991, 3rd Reference Catalogue of Bright Galaxies. Springer-Verlag, New York (RC3)

Devereux N.A., 1987, ApJ 323, 91

Draine B.T., Lee H.M., 1984, ApJ 285, 89

Dultzin-Hacyan D., 1997, Rev. Mex. Astron. Astrofis. SC 6

Dultzin-Hacyan D., 1995, Rev. Mex. Astron. Astrofis. SC 3, 31–37

Elmegreen D.M., Elmegren B.G., 1996, to be published in the AJ, June 1996

Gallagher J.S., Wirth A., 1980, ApJ 241, 567

Genzel R., Weitzel L., Tacconi-Gazman L.E., et al., 1995, ApJ 444, 129

Giuricin G., Mardirossian F., Mezzetti M., 1995, ApJ 446, 550

Granato G.L., Danese L., 1994, Mon. Notes R. Astron. Soc. 268, 235

Granato G.L., Danese L., Francheschini A., 1996, ApJ 460, L11

Haniff C.A., Wilson A.S., Ward M.J., 1988, ApJ 334, 104

Heckman T., 1990, In: Sulentic J.W., Keel W.C., Telesco C.M. (eds.) IAU Colloquium 124, Paired and Interacting Galaxies. NASA Conf.Publication 3098, p. 359

Heckman T., 1991, In: Leitherer N.R., Walborn T.M., Heckman C.A., Norman C.A. (eds.) Proc. Conf. Massive Stars in Starbursts. Cambridge University Press, Cambridge, p. 289

Ho L.C., Filippenko A.V., Sargent W.L.W., 1997, ApJS 112, 315 (HFS97)

Huchra J.P., Wyatt W.F., Davis, 1982, AJ 87, 1628

Jockers K., 1992, Astronomische Gesellschaft Abstr. Ser. No. 7, P 108, 184

Krugel E., Chini R., Kreysa E., Sherwood W.A., 1988, A&A 190, 47

Lonsdale C.J., Lonsdale C.J., Smith H.E., 1992, ApJ 391, 629 (LLS92)

Miley G.K., Neugebauer G., Soifer B.T., 1985, ApJ 293, L11

Mouri H., Taniguchi Y., 1992, ApJ 386, 68

Mulchaey J.S., Wilson A.S., Tsvetanov Z., 1996, ApJS 102, 309 (MWT96)

Norman C.A., 1987, In: Thuan T.X., Montmerle T., Tran J.T. (eds.) Starbursts and Galaxy Evolution. XXII Moriond Meeting, Editions Frontiëres, p. 483

Perez-Fournon L., Wilson A.S., 1990, ApJ 356, 456

Pogge R.W., 1989, ApJ 345, 730

Rowan-Robinson M., Crawford J., 1989, MNRAS 238, 523

Scoville N., Soifer B.T., 1991, In: Leitherer C., Walborn N.R., Heckman T.M., Norman C.A. (eds.) Proc. Conf. Massive Stars in Starbursts. Cambridge University Press, Cambridge, 233

Scoville N., Sargent A.I., Sanders D., Soifer B.T., 1991, ApJ 366, L5

Scoville N., Hibbard J.E., Yun M.S., van Gorkom J.H., 1994, In: Shlosman I.(ed.) Mass Transfer Induced Activity in Galaxies. Cambridge University Press, 191

Spitzer L. Jr., 1978, Physical Processes in the Interstellar Medium. Princeton University Observatory

Storci-Bergmann T., Rodriguez-Ardila A., Schnidt H.R., Wilson A.S., Baldwin J.P., 1996, ApJ 472, 83

Taniguchi Y., Sato Y., Kawara K., Murayama T., Mouri H., 1997, A&A 318, L1

Telesco C.M., Beclin E.E., Wynn-Williams C.G., Harper H.D.A., 1984, ApJ 282, 427

Telesco C.M., Dressel L.L., Wolstencroft R.D., 1993, ApJ 414, 120

Tsvetanov Z., Walsh J.R., 1992, ApJ 386, 485

van Driel W., Buta R.J., 1991, A&A 245, 7

Wada K., Habe A., 1992, MNRAS 258, 82

Wada K., Habe A., 1995, MNRAS 277, 433

Whittle M., 1992, ApJS 79, 49

Young J.S., Devereux N.S., 1991, ApJ 373, 414